Targeting the late component of the cardiac L-type Ca^{2+} current to suppress early afterdepolarizations

Roshni V. Madhvani,[1]* Marina Angelini,[1]* Yuanfang Xie,[7] Antonios Pantazis,[1] Silvie Suriany,[1] Nils P. Borgstrom,[5] Alan Garfinkel,[2,4,5] Zhilin Qu,[2,5] James N. Weiss,[2,3,5] and Riccardo Olcese[1,3,5,6]

[1]Division of Molecular Medicine, Department of Anesthesiology, [2]Department of Medicine (Cardiology), [3]Department of Physiology, [4]Department of Integrative Biology and Physiology, [5]Cardiovascular Research Laboratory, and [6]Brain Research Institute, David Geffen School of Medicine at University of California, Los Angeles, Los Angeles, CA 90095
[7]Department of Pharmacology, University of California, Davis, Davis, CA 95616

Early afterdepolarizations (EADs) associated with prolongation of the cardiac action potential (AP) can create heterogeneity of repolarization and premature extrasystoles, triggering focal and reentrant arrhythmias. Because the L-type Ca^{2+} current ($I_{Ca,L}$) plays a key role in both AP prolongation and EAD formation, L-type Ca^{2+} channels (LTCCs) represent a promising therapeutic target to normalize AP duration (APD) and suppress EADs and their arrhythmogenic consequences. We used the dynamic-clamp technique to systematically explore how the biophysical properties of LTCCs could be modified to normalize APD and suppress EADs without impairing excitation–contraction coupling. Isolated rabbit ventricular myocytes were first exposed to H_2O_2 or moderate hypokalemia to induce EADs, after which their endogenous $I_{Ca,L}$ was replaced by a virtual $I_{Ca,L}$ with tunable parameters, in dynamic-clamp mode. We probed the sensitivity of EADs to changes in the (a) amplitude of the noninactivating pedestal current; (b) slope of voltage-dependent activation; (c) slope of voltage-dependent inactivation; (d) time constant of voltage-dependent activation; and (e) time constant of voltage-dependent inactivation. We found that reducing the amplitude of the noninactivating pedestal component of $I_{Ca,L}$ effectively suppressed both H_2O_2- and hypokalemia-induced EADs and restored APD. These results, together with our previous work, demonstrate the potential of this hybrid experimental–computational approach to guide drug discovery or gene therapy strategies by identifying and targeting selective properties of LTCC.

INTRODUCTION

Early afterdepolarizations (EADs) are arrhythmogenic membrane potential oscillations that occur before repolarization of the cardiac action potential (AP) is complete. Although the mechanistic link between EADs in single cells and triggered arrhythmias in the heart is still a subject of intense investigation (Wit and Rosen, 1983; Rosen, 1988; Antzelevitch and Sicouri, 1994; El-Sherif et al., 1996; Yan et al., 2001; Xie et al., 2010; Yang et al., 2010), it is firmly established that EADs are capable of triggering fatal arrhythmias such as polymorphic ventricular tachycardia, torsade de pointes, and ventricular fibrillation (Yan et al., 2001; Choi et al., 2002; Wu et al., 2002; Antzelevitch, 2007; Bapat et al., 2012), which often exhibit a mixture of focal and reentrant mechanisms (Asano et al., 1997; Sato et al., 2009; Weiss et al., 2010; Chang et al., 2012). Not only are EADs capable of generating triggered activity to produce focal arrhythmias, but they are also associated with a prolonged AP duration (APD). Thus, they can markedly increase dispersion of refractoriness in tissue, predisposing to initiation of reentry (Sato et al., 2009; Weiss et al., 2010; Chang et al., 2012).

The onset of EADs (i.e., the reversal of the normal repolarization phase of the AP) occurs within a range of the membrane potentials where the steady-state activation and inactivation curves of the L-type Ca^{2+} current ($I_{Ca,L}$) overlap, known as the $I_{Ca,L}$ window current region (January et al., 1988). Within this membrane potential range, $I_{Ca,L}$ reactivation plays a key role in reversing the normal repolarization phase during EAD formation (January et al., 1988). Although other ionic currents also participate in EAD formation, a regenerative inward current such as $I_{Ca,L}$ is required for EADs to propagate in the tissue (Zeng and Rudy, 1995; Chang et al., 2012). Using the dynamic-clamp technique (Dorval et al., 2001) in isolated rabbit ventricular myocytes, we recently demonstrated that EADs are highly sensitive to subtle changes in the half-activation or half-inactivation potentials of $I_{Ca,L}$, suggesting that a reduction of the $I_{Ca,L}$ window current may represent an effective maneuver to

*R.V. Madhvani and M. Angelini contributed equally to this paper.
Correspondence to Riccardo Olcese: rolcese@ucla.edu

Abbreviations used in this paper: AP, action potential; APD, AP duration; EAD, early afterdepolarization; $I_{Ca,L}$, L-type Ca^{2+} current; VDI, voltage-dependent inactivation.

The Rockefeller University Press $30.00
J. Gen. Physiol. Vol. 145 No. 5 395–404
www.jgp.org/cgi/doi/10.1085/jgp.201411288

suppress EADs and normalize APD without blocking the early peak $I_{Ca,L}$ required to maintain a normal excitation–contraction coupling (Madhvani et al., 2011). The dynamic clamp is a powerful technique that allows one to introduce a model conductance, such as $I_{Ca,L}$, with programmable properties into a cell in real time to study its effects on AP characteristics (Fig. 1 E). The proof-of-concept provided by our initial study (Madhvani et al., 2011) prompted us to perform a comprehensive analysis of biophysical parameters influencing the time- and voltage-dependent properties of the window (late) $I_{Ca,L}$ to identify whether additional parameters could be modified to suppress EAD formation and normalize APD. Accordingly, we systematically investigated the slopes of the voltage dependence of activation and inactivation, the noninactivating (or very slowly inactivating) late pedestal current, and the time constants of activation and inactivation, which shape the $I_{Ca,L}$ window current (Fig. 1, A and C) during the cardiac AP.

The results demonstrate that of all the $I_{Ca,L}$ biophysical parameters explored in this and previous work (Madhvani et al., 2011), three stand out as highly effective targets both to suppress EAD formation and normalize APD to reduce dispersion of repolarization: the half-activation and half-inactivation potentials and the noninactivating pedestal current. Collectively, these findings provide a drug discovery target to search for new antiarrhythmic agents to suppress EAD-mediated arrhythmias. Moreover, this study recapitulates a novel hybrid experimental–computational approach incorporating the dynamic-clamp technique to predict how subtle alterations in biophysical properties of ionic currents such as $I_{Ca,L}$ affect cardiac electrophysiology and arrhythmogenic phenomena.

MATERIALS AND METHODS

Ethical approval

All animal-handling protocols were approved by the UCLA Institutional Animal Care and Use Committee and conformed to the Guide for the Care and Use of Laboratory Animals published by the US National Institutes of Health.

Electrophysiology

3–4-mo-old New Zealand male rabbits were euthanized by an intravenous injection of 1,000 U heparin sulfate and 100 mg/kg sodium pentobarbital; adequacy of anesthesia was confirmed by the lack of pedal withdrawal reflex, corneal reflex, and motor response to pain stimuli. Ventricular myocytes were dissociated using a retrograde Langendorff perfusion system as described previously (Chen et al., 2003), and washed and bathed in Tyrode's solution containing (mM): 136 NaCl, 5.4 KCl, 1 $MgCl_2$, 0.33 NaH_2PO_4, 1.8 $CaCl_2$, 10 glucose, and 10 HEPES, adjusted to pH 7.4. The intracellular solution contained (mM): 110 K-aspartate, 30 KCl, 5 NaCl, 10 HEPES, 0–0.1 EGTA, 5 MgATP, 5 creatine phosphate, and 0–0.05 cAMP adjusted to pH 7.2. EADs were induced by perfusing 600 µM H_2O_2 or reducing the external $[K^+]$ from 5.4 to 2.7 mM. All chemicals were purchased from Sigma-Aldrich. All electrophysiological recordings were performed using an Axopatch 200B amplifier (Axon Instruments) in current-clamp mode at ∼34–36°C using 1–2-MΩ borosilicate pipettes (Warner Instruments). Data were acquired and analyzed using custom-made software (G-Patch; Analysis).

Dynamic clamp

Under dynamic-clamp mode, a virtual $I_{Ca,L}$ with the properties of the native $I_{Ca,L}$ is injected into the myocytes. To predict $I_{Ca,L}$ and its Ca^{2+}-dependent inactivation, our ventricular myocyte model also computes intracellular Ca^{2+} cycling. To predict the spatiotemporal distribution of intracellular calcium, average $[Ca^{2+}]$ was computed in four different cellular compartments, namely the "submembrane space" in proximity of the sarcolemma (C_s), the "bulk myoplasm," the "junctional SR," and "network SR," as described previously (Shiferaw et al., 2003; Mahajan et al., 2008; Madhvani et al., 2011). The main Ca^{2+}-regulated ionic conductance was also included in the model, i.e., the fast sodium current (I_{Na}), the Na^+/K^+ pump current (I_{NaK}), the Na^+/Ca^{2+} exchange current (I_{NCX}), and the Ca^{2+}-dependent slow component of the delayed rectifier potassium channel (I_{Ks}). Calcium-modulated currents sense the $[Ca^{2+}]$ at submembrane space (C_s), which is higher than the global $[Ca^{2+}]$ (C_i) (Weber et al., 2002). The average C_s is used to calculate Ca^{2+}-dependent inactivation in the $I_{Ca,L}$ formulation, whereas C_i was acquired during the course of the experiments to predict the amplitude and shape of the Ca_i transient.

In brief, the Ca^{2+} flux into the cell caused by $I_{Ca,L}$ is given by:

$$J_{Ca} = g_{Ca} Po i_{Ca} \tag{1}$$

$$i_{Ca} = \frac{4P_{Ca}VmF^2}{RT}\frac{Cse^{2a} - 0.341[Ca^{2+}]_o}{e^{2a}-1}, \tag{2}$$

where C_s is the submembrane Ca^{2+} concentration in units of millimolar, P_{Ca} (0.00054 cm/s) is the Ca^{2+} channel permeability, V_m is the membrane potential, F is the Faraday constant, and T is temperature.

P_O was formulated as:

$$Po = d \cdot f \cdot q, \tag{3}$$

where d is the voltage-dependent activation gate, f is the VDI gate, and q is the Ca^{2+}-dependent inactivation gate. The steady states of these gating variables as functions of the membrane potential (V_m) were formulated as follows:

$$d_\infty = \frac{1}{1.0 + \exp\left(-\left(Vm - dhalf\right)/dslope\right)} \tag{4}$$

$$f_\infty = \frac{1 - pdest}{1.0 + \exp\left(\left(Vm - fhalf\right)/fslope\right)} + pdest \tag{5}$$

$$q_\infty = \frac{1}{1.0 + \left(\frac{Cs}{cst}\right)^\gamma} \tag{6}$$

$$\tau_d = \frac{d_\infty\left(1 - \exp\left(-Vm - \left(dhalf + a_1\right)\right)\right)}{a_2\left(dslope + a_2\right)\left(Vm - \left(dhalf + a_1\right)\right)} \tag{7}$$

$$\tau_f = \frac{1}{b_1 \exp\left(-b_2\left(Vm - \left(fhalf + b_3\right)\right)^2\right) + b_4}, \tag{8}$$

where *dhalf* and *fhalf* are the potentials at half-maximum of activation and inactivation, respectively; *pdest* is the noninactivating pedestal of the inactivation gate; and *dslope/fslope* are the steepness of the voltage dependence of activation and inactivation, respectively. These two parameters are called slope factors (k) in this study, and are related to effective charge (z) by RT/z, where R is the gas constant and T is temperature. *Cs* is the submembrane $[Ca^{2+}]$; *Cst* is the affinity for Ca^{2+} of the inactivation gate; τ_d and τ_f are the time constants of the *d* gate and the *f* gate, respectively; and a_1, a_2, b_1, b_2, b_3, and b_4 are additional factors used for fitting. The control parameters in the $I_{Ca,L}$ formulation were determined by fitting formulated current to experimental nifedipine-sensitive $I_{Ca,L}$ records (Madhvani et al., 2011) using Berkeley Madonna and then implemented for dynamic clamp in RTXI (http://www.rtxi.org; Lin et al., 2010). In each experiment, as soon as the whole-cell configuration was obtained, the cell capacitance of the myocyte was measured (usually ranging within 100–150 pF) and entered as one of the parameters of the dynamic-clamp model to scale the computed $I_{Ca,L}$ accordingly to the cell size. The sampling/computation frequency was 10 kHz.

In some experiments, 10% of the computed slow component of the delayed rectifier K^+ current (I_{Ks}) was injected together with $I_{Ca,L}$. I_{Ks} was modeled as in Mahajan et al. (2008).

Data analysis

APD at 90% repolarization (APD_{90}) was calculated using custom-made software, whereas EAD amplitude was calculated manually by measuring the difference in V_m from the local minimum where dV/dt is 0 to the peak of the EAD where dV/dt is also 0. In APs that displayed multiple EADs, only the EAD with the largest voltage excursion was included in the analysis. EAD occurrence is reported as the percentage of APs that displayed at least one EAD. Error bars show the SEM.

Computer simulations

Single-cell AP simulations were produced using the rabbit ventricular myocyte AP model developed by Mahajan et al. (2008), with some modifications. For details, see the supplemental text.

Online supplemental material

Online supplemental figures show the effects of varying the slope (k) of the steady-state inactivation curve (Fig. S1) and the predicted Ca_i transient before and after reduction of $I_{Ca,L}$ pedestal (Fig. S2) under the dynamic clamp. Fig. S3 demonstrates that the reduction of $I_{Ca,L}$ noninactivating component effectively suppressed EADs under hypokalemia condition. Fig. S4 shows results from computer simulation using a model of rabbit myocytes with properties of M, endo, and epi cell layers. Table S1 reports the mean values for EAD occurrence and APD_{90} for different $I_{Ca,L}$ activation and inactivation time constants. Table S2 shows the biophysical parameters of $I_{Ca,L}$ in the dynamic-clamp model for control, H_2O_2, and hypokalemia conditions. Tables S3 and S4 provide parameter values for maximal ionic conductances used in the computer simulation using a model of rabbit AP with properties of epi, endo, and M cell layers. The online supplemental material is available at http://www.jgp.org/cgi/content/full/jgp.201411288/DC1.

RESULTS

Sensitivity of EAD occurrence to the noninactivating component of $I_{Ca,L}$

In our previous study (Madhvani et al., 2011), we demonstrated that modest shifts (<5 mV) in the half-activation and half-inactivation potentials of $I_{Ca,L}$, which reduce the overlap between steady-state activation and inactivation curves (i.e., the window current region; Fig. 1 A), potently suppressed EADs, without adversely altering APD or the computed intracellular Ca_i transient. However, other parameters also affect the $I_{Ca,L}$ window current and its ability to contribute to EAD formation. Using dynamic clamp, we have explored the extent to which the other properties affecting activation and inactivation contribute to EAD formation.

To induce an EAD regimen, myocytes were paced at 5-s cycle length under current-clamp mode and superfused with 600 µM H_2O_2 until EADs appeared consistently. The native $I_{Ca,L}$ was then blocked with 20 µM nifedipine, which eliminated EADs and markedly shortened the APD (Fig. 1 D). Next, the dynamic clamp was

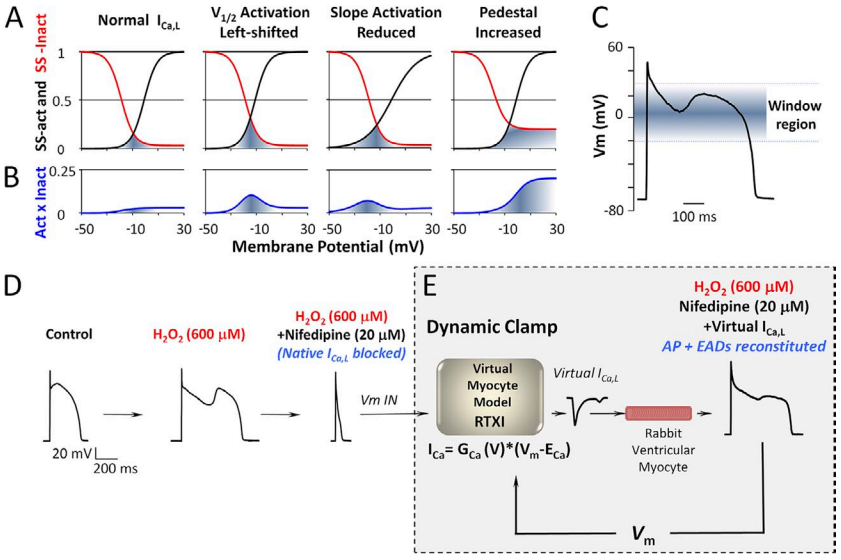

Figure 1. The $I_{Ca,L}$ window current region and the experimental design for dynamic clamp. (A) Changing steady-state biophysical properties of $I_{Ca,L}$, such as the half-activation potential ($V_{1/2}$ activation), the slope of the activation curve, or the noninactivating pedestal of the inactivation curve has a large impact on the $I_{Ca,L}$ window region, i.e., the area (shaded) subtended by the intersection of the voltage-dependent activation and inactivation curves. (B) The window region bounded by the product of the steady-state activation and steady-state inactivation curves (SS-act × SS-inact). (C) A typical rabbit ventricular myocyte AP after exposure to 600 µM H_2O_2, displaying a large-amplitude EAD. EADs often occur within the range of membrane potentials defined by the window current (around −30 to 20 mV). (D) Representative APs for the experimental protocol used in this study: cardiac myocytes (paced at 5 s; left) were exposed to 600 µM H_2O_2 to induce EADs (middle). The addition of 20 µM nifedipine blocked the native $I_{Ca,L}$ (right). Under dynamic clamp (E), the myocyte membrane potential is fed into the model, which computes and injects a virtual $I_{Ca,L}$ into the cell in real time and reconstitutes EADs in the continuous presence of H_2O_2.

engaged to replace the native $I_{Ca,L}$ (blocked by nifedipine) by injecting, in real time, a $I_{Ca,L}$ computed from Eqs.1–8, causing EADs to reappear (Fig. 1 E). The membrane potential of the myocyte was continuously sampled and fed into the dynamic-clamp model, creating a bidirectional relationship between the cell and the model, in real time (Fig. 1 E). The injected $I_{Ca,L}$ had the properties of the native $I_{Ca,L}$ in the presence of 600 µM H_2O_2 (Madhvani et al., 2011). Importantly, all dynamic-clamp experiments were performed in the continuous presence of H_2O_2 or hypokalemia, maintaining a pathological state that resulted in EAD formation.

The inactivation of $I_{Ca,L}$ caused by voltage- and Ca^{2+}-dependent mechanisms (voltage-dependent inactivation, VDI, and Ca^{2+}-dependent inactivation, CDI, respectively) (Catterall, 2000) is incomplete during the time course of an AP. This noninactivating component was previously found to be elevated (from ∼3 to ∼10% of the peak current) in myocytes exposed to an EAD-promoting regimen (H_2O_2) (Madhvani et al., 2011), suggesting that this residual current contributes to EAD formation by effectively increasing $I_{Ca,L}$ window region (Fig. 1, A and B). Motivated by these pieces of evidence, we directly probed EAD sensitivity to changes in the amplitude $I_{Ca,L}$ noninactivating component (pedestal) (Rose et al., 1992; Qu and Chung, 2012). As demonstrated in Fig. 2, after inducing EADs in a myocyte by H_2O_2 superfusion (Fig. 2 B), the EADs were abolished by nifedipine (Fig. 2 C) and reconstituted by injecting a virtual $I_{Ca,L}$ (Fig. 2 D). Under these conditions, APs were markedly prolonged, displaying a consistent EAD regimen, although with oscillations that tended to be smaller in amplitude than the ones typically observed experimentally (Fig. 2). Because nifedipine abolishes the Ca_i transient, which is important for activating I_{Ks} (Tohse, 1990; Nitta et al., 1994), we compensated by adding 10% of the computed I_{Ks} to the injected current. This maneuver reduced the voltage plateau into a range promoting greater $I_{Ca,L}$ reactivation and larger EAD oscillations (Fig. 2 E), more closely resembling H_2O_2-induced EADs before nifedipine blockade. The reduction of the $I_{Ca,L}$ pedestal from 10 to 4% of the peak completely suppressed EAD occurrence and shortened the APD_{90} from 1,090 ± 80 ms to 197 ± 3 ms (Figs. 2 F and 3) whether or not EAD amplitude was increased by adding I_{Ks}. Importantly, the reduction of the $I_{Ca,L}$ pedestal suppresses the EAD regimen without attenuating the amplitude of the predicted Ca_i transient (Fig. S2).

These results indicate that the reduction of the noninactivating $I_{Ca,L}$ pedestal current can be an effective therapeutic strategy to suppress EADs.

Sensitivity of EADs to the steepness of steady-state activation and inactivation curves

Another set of parameters affecting the $I_{Ca,L}$ window current region are the steepness of the voltage dependence of activation and inactivation. However, modification of either parameter did not completely suppress EADs, nor did it restore normal APD, in contrast to the consequences of noninactivating pedestal current reduction. After reconstitution of the EADs with dynamic clamp in the presence of H_2O_2 in the superfusate, we first examined the effects of altering the slope factor (k) of the voltage dependence of activation from 4 mV (effective valence, $z = 5.7\ e^0$) to 1 mV ($z = 25.6\ e^0$) or 8 mV ($z = 3.2\ e^0$) to increase or decrease, respectively, the steepness of

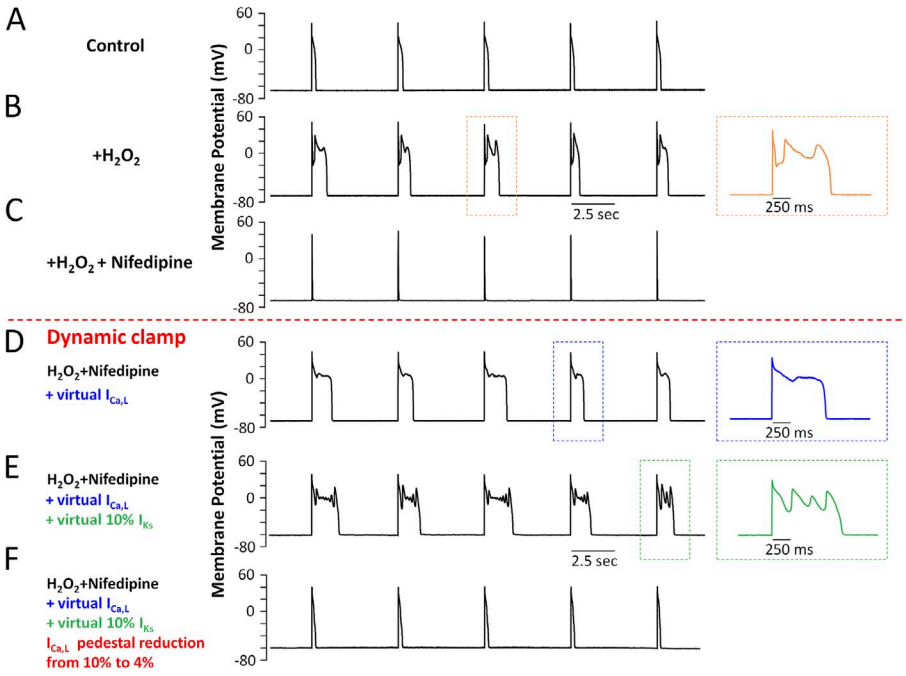

Figure 2. Potent suppression of EAD by reduction of the noninactivating (pedestal) $I_{Ca,L}$ component. (A) APs recorded from rabbit ventricular myocytes at a pacing cycle length of 5 s at 35–37°C in control conditions. (B) Perfusion of 600 µM H_2O_2 to the bath solution–induced EADs within 5–10 min. (C) The addition of 20 µM nifedipine blocked the native $I_{Ca,L}$, shortened APD, and abolished EADs. (D) Under dynamic clamp and in the presence of H_2O_2, we evaluated the injection of virtual $I_{Ca,L}$ or (E) the combination of $I_{Ca,L}$ plus 10% of the computed I_{Ks}. Note that both conditions regenerate the EAD regimen, although the amplitude of the oscillations tended to be larger with the addition of 10% I_{Ks}. (F) Varying a single $I_{Ca,L}$ parameter, the noninactivating (pedestal) component completely abolished EADs, despite the presence of H_2O_2.

the voltage dependence of activation (Fig. 4 A). We found that, at greater steepness, EAD amplitudes decreased from 5.6 ± 0.7 mV to 3.1 ± 1 mV (for k = 2 mV, $z = 12.8\ e^0$) or 2.6 ± 0.8 mV (k = 1 mV, $z = 25.6\ e^0$) (Fig. 4, B and C). Also, for the steepest slope (k = 1 mV, $z = 25.6\ e^0$), the APD became prolonged such that, in some cases, the AP failed to repolarize before the next pacing stimulus (APD > 5 s) (Fig. 4 B). Conversely, when the effective charge of the activation curve was reduced from k = 4 mV ($z = 6.4e^0$) to k = 6 mV ($z = 4.3e^0$), EAD amplitude increased from 5.6 ± 0.7 mV to 12.3 ± 1.4 mV (Fig. 4, B and C). This effect was even more pronounced for k = 8 mV ($z = 3.2e^0$), such that the mean EAD amplitude increased to 21.4 ± 2 mV (Fig. 4, B and C), although no significant changes in percentage of APs with EADs were observed (Fig. 4 D), and APD_{90} remained prolonged for these maneuvers (Fig. 4 E).

We also investigated the effects of changing the slope of the voltage dependence of inactivation (Fig. S1 A) by increasing or decreasing the effective charge to k = 1 mV ($z = 25.6\ e^0$) or k = 8 mV ($z = 3.2\ e^0$), respectively. We did not observe a significant difference in either EAD amplitude or in percentage of APs with EADs (Fig. S1, C and D). APD_{90} prolonged from 1,104 ± 319 ms to 3,140 ± 771 ms (Fig. S1, B and E) as the steepness of the inactivation curve was reduced from k = 4 mV ($z = 6.4\ e^0$) to k = 8 mV ($z = 3.2\ e^0$) (Fig. S1 A).

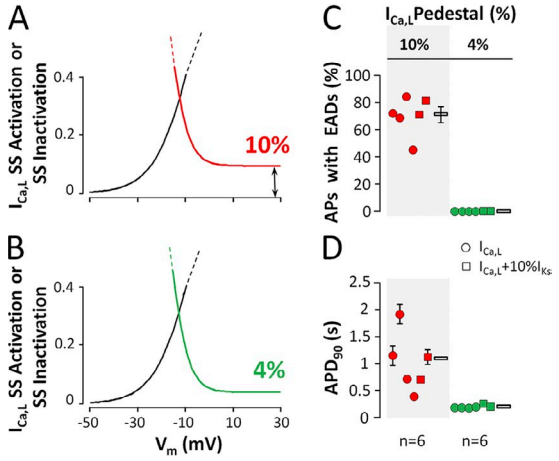

Figure 3. A reduction in the noninactivating (pedestal) $I_{Ca,L}$ potently suppresses EADs and restores APD. (A and B) Enlarged view of the steady-state activation and inactivation curves of $I_{Ca,L}$ shows changes made to the noninactivating component (pedestal). Under dynamic clamp and in the presence of H_2O_2, we evaluated the effect of lowering the noninactivating pedestal from 10% (A) to 4% of the peak current (B). (C) The proportion of APs displaying EADs under two different pedestal amplitudes. (D) APD_{90} under two different pedestal amplitudes. Note that lowering the pedestal current to 4% eliminated EADs and restored a normal APD when either $I_{Ca,L}$ only (circles) or $I_{Ca,L}$ plus 10% I_{Ks} (squares) was injected. The means for all experiments are plotted as open rectangles ($n = 6$ from six rabbits). Error bars indicate SEM.

Sensitivity of EADs to the kinetics of $I_{Ca,L}$ activation and inactivation

We next studied the effects of altering the time constants of $I_{Ca,L}$ activation and inactivation on EAD formation during oxidative stress. Overall, we found that changes in the rates of $I_{Ca,L}$ activation or inactivation by up to 10-fold had limited efficacy at suppressing EADs induced by H_2O_2 (Figs. 5 and 6).

Specifically, in the presence of H_2O_2, slowing $I_{Ca,L}$ activation by twofold ($\tau_d \times 2$) maintained an average APD_{90} of 1,550 ± 130 ms, and EAD occurrence remained high at 91 ± 4% (Table S1). A 10-fold slowing of $I_{Ca,L}$ activation ($\tau_d \times 10$) prolonged APD_{90} from 1,376 ± 200 ms to 2,711 ± 548 ms, whereas EAD occurrence increased from 76 ± 8% to 100% of APs. Conversely, increasing the rate of $I_{Ca,L}$ activation by twofold ($\tau_d \times 0.5$; Table S1) or by 10-fold ($\tau_d \times 0.1$) had only a modest impact on both APD_{90} (1,122 ± 126 ms or 1,104 ± 165 ms) and EAD occurrence (79 ± 15% or 77 ± 10%), respectively (Fig. 5 and Table S1).

When the rate of VDI in the dynamic-clamp model was increased by twofold ($\tau_f \times 0.5$), neither APD_{90} (from

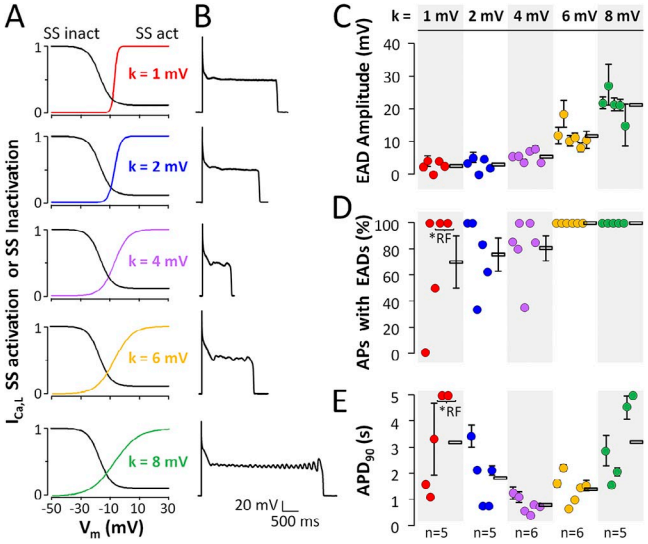

Figure 4. EAD amplitude is sensitive to changes in the slope of the steady-state voltage dependence of activation of $I_{Ca,L}$. (A) Under dynamic clamp and in the presence of H_2O_2, we evaluated the effects of varying the slope factor (k) of the steady-state activation curve. Steady-state inactivation properties were unperturbed, whereas the slope of the steady-state activation curve was varied under dynamic clamp from k = 1 mV to k = 8 mV. The set of curves in the center, k = 4 mV, corresponds to the native $I_{Ca,L}$ modified by H_2O_2. (B) Representative APs obtained for each k value studied, displaying EADs. For each value of k tested, the mean EAD amplitude (C), EAD occurrence (D), and APD_{90} (E) are shown. Data from individual cells are shown as closed circles, and the means for all experiments are plotted as an open rectangles ($n = 5$–6 cells from five to six rabbits). Error bars indicate SEM. *, instances when the AP failed to repolarize before the next pacing stimulus are reported as RF (repolarization failure). Note that EAD amplitude grows as k is increased (slope becomes shallower).

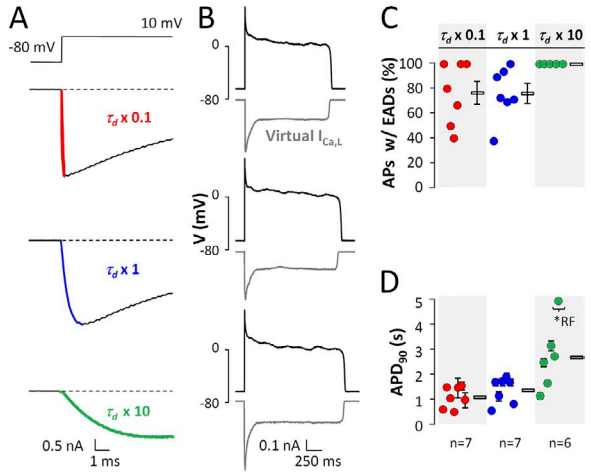

Figure 5. Time constant of $I_{Ca,L}$ activation has a limited effect on H_2O_2-induced EADs. (A) $I_{Ca,L}$ model outputs in response to depolarizing pulses from −80 to 10 mV using three different time constants of activation (τ_d). (B) Representative APs recorded under dynamic-clamp conditions from myocytes in which the endogenous $I_{Ca,L}$ was replaced with a virtual $I_{Ca,L}$ with modified activation time constants. The injected virtual $I_{Ca,L}$ in dynamic clamp is shown in gray under each AP trace. Increasing or decreasing $I_{Ca,L}$ activation rate by a factor of 10 did not significantly shorten APD or suppress EADs. For each value of τ_d tested, EAD occurrence (C) and APD_{90} (D) are shown. Data from individual cells are shown as closed circles, and the means for all experiments are plotted as open rectangles ($n = 7$ from five to six rabbits). Note that in all cases, APD_{90} remained prolonged (≥500 ms). Error bars indicate SEM. *, instances when the AP failed to repolarize before the next pacing stimulus are reported as RF (repolarization failure).

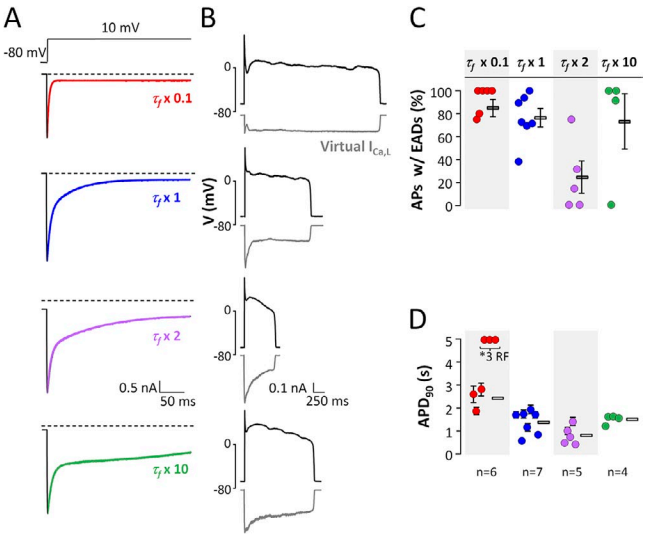

Figure 6. $I_{Ca,L}$ time constant of inactivation has limited efficacy for suppressing EADs induced by H_2O_2. (A) $I_{Ca,L}$ model outputs in response to depolarizing pulses from −80 to 10 mV using four different time constants of inactivation (τ_f). (B) Representative APs recorded under dynamic-clamp conditions from myocytes in which the endogenous $I_{Ca,L}$ was replaced with a virtual $I_{Ca,L}$ with modified inactivation time constants. The injected virtual $I_{Ca,L}$ in dynamic clamp is shown in gray under each AP trace. For each value of τ_f tested, EAD occurrence (C) and APD_{90} (D) are shown. Data from individual cells are shown as closed circles, and the means for all experiments are plotted as open rectangles ($n = 4$–7 from three to five rabbits). A limited favorable effect on EAD occurrence was observed for decreasing τ_f by a factor of 2; however, on average, APs remained prolonged (>500 ms). Error bars indicate SEM. *, instances when the AP failed to repolarize before the next pacing stimulus are reported as RF (repolarization failure).

1,376 ± 200 ms to 1,838 ± 435 ms) nor EAD occurrence (from 76 ± 8% to 70 ± 16%) was dramatically altered (Table S1). Accelerating VDI by 10-fold ($\tau_f \times 0.1$; Fig. 6 A) increased APD_{90} (to 2,433 ± 290 ms) (Fig. 6 D), and EAD occurrence remained high (85 ± 8%; Fig. 6 C and Table S1). Conversely, decreasing the rate of VDI by two-fold ($\tau_f \times 2$; Fig. 6 A) reduced EAD occurrence to 24 ± 14% (Fig. 6 C), but APD_{90} remained prolonged (802 ± 183 ms; Fig. 6 D). Decelerating inactivation by 10-fold ($\tau_f \times 10$), on the other hand, did not reduce EAD occurrence (73 ± 24% of APs), and significantly prolonged APD_{90} (1,506 ± 102 ms; Fig. 6, C and D, and Table S1).

Reduction of $I_{Ca,L}$ noninactivating component is effective at suppressing EADs under hypokalemia, another EAD-favoring condition

In addition to our previously reported finding that EADs could be suppressed, and the APD could be normalized, by modest shifts of the half-voltage of steady-state activation or inactivation (Madhvani et al., 2011), the present results indicate that suppressing the noninactivating $I_{Ca,L}$ pedestal current is an effective strategy, whereas the modification of other biophysical parameters affecting the steepness or kinetics of activation and inactivation is unreliable. To ascertain whether reducing $I_{Ca,L}$ pedestal is effective at suppressing EADs caused by a mechanism other than oxidative stress, we also examined its potency at suppressing hypokalemia-induced EADs. As shown previously (Sato et al., 2010), lowering extracellular [K^+] from 5.4 to 2.7 mM readily induced EADs within 5–10 min. Using the same dynamic-clamp approach, the endogenous nifedipine-sensitive current was replaced by a virtual $I_{Ca,L}$, the parameters of which were modified to simulate the effects of hypokalemia on the native $I_{Ca,L}$ (Table S2). The virtual $I_{Ca,L}$ reconstituted EADs were greatly suppressed ($n = 3$) or completely abolished ($n = 2$) by reducing the pedestal component of the virtual $I_{Ca,L}$ from 5% to ≤0.5% (Fig. S3, C and D).

Effects of noninactivating pedestal of $I_{Ca,L}$ on simulated EADs in epicardial, endocardial, and M cell types

Across the ventricular wall, there are regional differences in the ionic basis underlying ventricular APs (Antzelevitch et al., 1991; Antzelevitch and Sicouri, 1994). To explore how these regional differences affect the ability of a therapeutic reduction in the $I_{Ca,L}$ pedestal to suppress EADs, we modified the rabbit ventricular AP model to simulate epicardial, endocardial, and M cell

layer APs, respectively. When paced at a 5-s cycle length under control conditions, with a 3% $I_{Ca,L}$ pedestal current (Fig. S4 A), APD_{90} averaged 229, 258, and 268 ms for the epicardial, endocardial, and M cells, respectively. We then simulated the effects of H_2O_2 as described above, including increasing the $I_{Ca,L}$ pedestal current to 6%. The APD_{90} prolonged to 540, 504, and 811 ms, respectively, and EADs appeared in all three cell types (Fig. S4 B). When the $I_{Ca,L}$ pedestal current was reduced to 0%, while maintaining all other H_2O_2 effects, APD_{90} shortened to 273, 293, and 309 ms, respectively, and EADs disappeared (Fig. S4 C). Thus, suppressing the $I_{Ca,L}$ pedestal current was effective at eliminating EADs regardless of transmural AP heterogeneity.

DISCUSSION

Although many ionic currents can contribute to EAD formation, reactivation of $I_{Ca,L}$ plays a central role in providing a regenerative inward current required for EADs to propagate, thereby causing triggered activity in multicellular tissue (January et al., 1988; January and Riddle, 1989). The main finding of the present study is that, even though H_2O_2 is likely to promote EADs by affecting multiple ionic currents such as late I_{Na} (Song et al., 2006), the modification of $I_{Ca,L}$ is sufficient to prevent EADs even in the presence of H_2O_2. Furthermore, this intervention does not diminish the amplitude of the predicted Ca_i transient (Fig. S2) and therefore is expected to maintain normal cell contractility. Conventional Ca^{2+} channel blockers such as nifedipine, which indiscriminately block both peak and window $I_{Ca,L}$, are highly effective at suppressing EADs (e.g., Fig. 1 D). However, by blocking peak $I_{Ca,L}$, these drugs also potently suppress excitation–contraction coupling, precluding clinical usefulness for EAD suppression.

In this study, we applied the dynamic-clamp technique to systematically evaluate the hypothesis that EADs

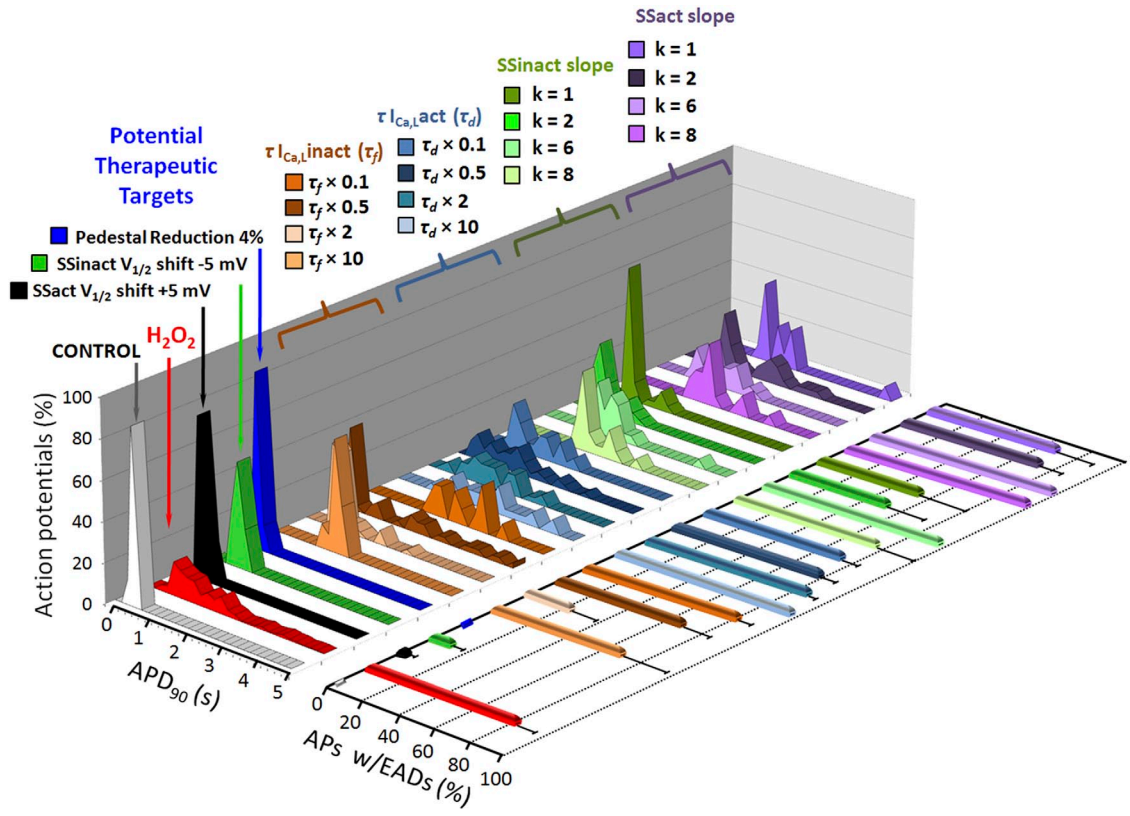

Figure 7. The effects of modification of $I_{Ca,L}$ time-dependent and steady-state biophysical properties on APD_{90} and EAD formation. 3-D plot showing the APD distribution for each experimental condition (n = 4–28 from 4–14 rabbits). The histograms show the percentage of APs that fall within 200-ms bins up to 5 s. APs in control conditions (white) have a narrow duration distribution with most APs ∼250 ms. Under dynamic clamp, in the presence of H_2O_2, the APD distribution broadens, with most APs longer than 1 s (red). Changes in the slopes of the steady-state activation (purple) or inactivation (green) curves, or the time constants of activation (cyan) or inactivation (brown), maintain broad APD distributions. A 6% reduction of the pedestal current (blue), a 5-mV leftward shift in the half-inactivation potential (olive), or a 5-mV rightward shift in the half-activation potential (black) restores APD distributions to around 250 ms (Madhvani et al., 2011). The corresponding EAD occurrence for each condition is shown plotted perpendicular to the z axis and on the same plane as the floor of the histogram. EAD occurrence is plotted as the percentage of APs with EADs in each experimental condition. In control conditions, no EADs are present (white bar). EAD occurrence is high for all maneuvers studied except for a reduction in the pedestal (blue bar), or favorable shifts in the half-inactivation (olive) and half-activation potentials (black).

can be suppressed by selectively targeting the biophysical properties regulating the $I_{Ca,L}$ window current. Fig. 7 summarizes the effects of the various parameter changes on both APD and EAD occurrence, illustrating that three parameter modifications (depolarizing shift of the half-activation potential, hyperpolarizing shift of the half-inactivation potential, and reduction of the pedestal current) both effectively suppress EADs and restore APD toward a normal value. From these findings, we predict that the ideal Ca^{2+} channel agent for suppressing EAD-mediated arrhythmias (drugs or genetic intervention) would leave peak $I_{Ca,L}$, hence excitation–contraction coupling, intact but selectively suppress late $I_{Ca,L}$ in the window region. An important novel contribution of the present study is the finding that the $I_{Ca,L}$ pedestal current has an equivalent promise to the half-activation and half-inactivation potentials as a novel anti-arrhythmic target to suppress EAD formation, which is robust across the spectrum of simulated transmural AP differences in the ventricular epicardial, M cell, and endocardial layers (Fig. S3). Moreover, it is effective for different mechanisms of EAD generation, as H_2O_2 primarily causes EADs by increasing inward currents including late I_{Na} and $I_{Ca,L}$ as a result of oxidative CaMKII activation (Ward and Giles, 1997; Xie et al., 2009; Wagner et al., 2011), whereas hypokalemia causes EADs by reducing K^+ conductances, i.e., I_{Kr}, and Na^+/K^+ ATPase activity, which in turn causes accumulation of intracellular Na^+ and Ca^{2+}. The finding that selective blockade of the $I_{Ca,L}$ pedestal has potent EAD-suppressing effects is particularly intriguing because of the precedent in Na^+ channels, in which selective blockers of the late Na^+ current (I_{Na}), which leave the peak I_{Na} intact, are already in clinical use (Karwatowska-Prokopczuk et al., 2013). Given the overall structural similarities between Na^+ and Ca^{2+} channels, the likelihood that analogous agents that selectively block late $I_{Ca,L}$ can also be identified seems high. Moreover, because late I_{Na} can also play an important role in EAD formation (Xie et al., 2009; Yang et al., 2012), we can further speculate that the combination of a late I_{Na} blocker with a late $I_{Ca,L}$ blocker might be a particularly efficacious anti-arrhythmic combination to prevent EAD-mediated arrhythmias.

The effects of modifying various $I_{Ca,L}$ parameters on the APD and EAD occurrence observed in this study can be understood in terms of the dynamical theory of EAD formation as a dual Hopf-homoclinic bifurcation (Tran et al., 2009; Qu et al., 2013). In this theory, the membrane voltage oscillations characterizing EADs depend critically on the amount of time that the membrane potential dwells in the window region during repolarization. This dwell time must be long enough for the growth rate of $I_{Ca,L}$ to overcome counterbalancing repolarizing currents such as I_{Ks}, thereby generating the upstroke of the EAD. As the membrane potential exceeds the voltage for peak $I_{Ca,L}$ ($\sim$0 mV), the diminishing amplitude of $I_{Ca,L}$ and voltage-dependent growth of I_{Ks} force the repolarization phase of the EAD, with this tug-of-war generating successive oscillations. Our results show that EAD amplitude is a function of the slope of the voltage dependence of $I_{Ca,L}$ activation (Fig. 4), consistent with the dynamical theory stating that membrane oscillations (EADs) occur because of instability of the $I_{Ca,L}$ in the window current voltage range via a Hopf bifurcation (Tran et al., 2009; Qu et al., 2013). EAD formation is more susceptible to interventions that limit the maximum steady-state amplitude that the late $I_{Ca,L}$ can achieve during repolarization (shifts in half-activation and half-inactivation potential and pedestal current) than to interventions that change the rate of growth (time constants of activation and inactivation) or shape of the window $I_{Ca,L}$ (slopes of inactivation and inactivation). Although EAD occurrence could be diminished with small changes in steady-state parameters (<5-mV shifts in half-activation and half-inactivation potential or reduction in the pedestal current; Fig. 7), kinetic parameters required order-of-magnitude changes to produce modest effects, often causing excessive changes in APD (Figs. 4–7 and S1).

Limitations and Implications

There are several limitations in this experimental–computational approach:

Rabbit versus human ventricular myocytes. This study was performed in rabbit ventricular myocytes, which differ in some respects from human myocytes. Although the results from this study need to be validated in human myocytes, previous studies have shown that the $I_{Ca,L}$ properties are generally similar in both species (Grandi et al., 2010; Verkerk et al., 2011), suggesting that suppression of $I_{Ca,L}$ noninactivating component could be an effective therapeutic strategy.

Virtual $I_{Ca,L}$. To study how the biophysical properties of $I_{Ca,L}$ affect EAD formation, it was required to replace the endogenous $I_{Ca,L}$ with a computed, "virtual" $I_{Ca,L}$ with tunable parameters under dynamic-clamp conditions. The current injected under the dynamic clamp, although incorporating Ca^{2+}-dependent inactivation in response to the virtual Ca_i transient in the model, did not trigger SR Ca^{2+} release in the myocytes. Thus, endogenous Ca^{2+}-sensitive currents in the myocyte, such as Na^+/Ca^{2+} exchange and I_{Ks}, were not activated. One consequence was that EADs reconstituted after virtual $I_{Ca,L}$ injection were smaller than before nifedipine blockade (Fig. 2): this could be corrected by injecting additional I_{Ks} via the dynamic clamp to simulate Ca^{2+}-induced activation of I_{Ks} (Fig. 2 E). Importantly, whether or not additional I_{Ks} were injected, reduction of the noninactivated pedestal was equally potent at suppressing EADs and restoring the APD.

Off-target effects of nifedipine. Our experimental approach required the full block of the endogenous $I_{Ca,L}$ to correctly evaluate the EAD sensitivity to the relatively small $I_{Ca,L}$ pedestal. We used 20 µM nifedipine, one of the most selective L-type Ca^{2+} channel blockers available. At the concentration used in this work, nifedipine may have had off-target effects, and possibly partially blocked I_{to} conductance (Gotoh et al., 1991). This effect may have contributed to the reduction of EAD amplitude, as observed in some of the experiments under dynamic clamp (e.g., Fig. 2 D); however, we were able to effectively restore EAD amplitude by the addition of a fraction of the computed I_{Ks} to the injected current (Fig. 2 E). We are confident that off-target effects of nifedipine have not biased the overall conclusion of this work, as the consequences of reducing $I_{Ca,L}$ pedestal current were also tested and confirmed in pure computer simulations, presented in Fig. S4.

Despite its limitations, we believe that this approach outlines a useful new strategy for drug discovery, potentially adaptable to high throughput screening of small molecules or genetic interventions, to identify new antiarrhythmic agents. In this context, the dynamic-clamp approach represents a powerful method to move beyond simple screening for indiscriminate ion channel blockers and toward identifying and targeting subtle and selective aspects of ion channel biophysics to guide drug discovery.

We thank the members of the Olcese, Weiss, Qu, Garfinkel, and Karagueuzian laboratories for constructive discussions during the development of the project. We are also grateful to Maurizio Carnesecchi for contributing analytical software.

This work was supported by the National Heart, Lung and Blood Institute of the National Institutes of Health (NIH; P01HL78931 and R01 HL103662 to J.N. Weiss, and NIH/NIGMS R01GM082289 to R. Olcese), American Heart Association (WSA) Predoctoral Fellowship (10PRE3290025 to R.V. Madhvani), American Heart Association (NCRP) Scientist Development Grant (14SDG20300018 to A. Pantazis), and the Laubisch and Kawata endowments (to J.N. Weiss).

The authors declare no competing financial interests.

Richard L. Moss served as editor.

Submitted: 10 September 2014
Accepted: 1 April 2015

REFERENCES

Antzelevitch, C. 2007. Ionic, molecular, and cellular bases of QT-interval prolongation and torsade de pointes. *Europace.* 9:iv4–iv15. http://dx.doi.org/10.1093/europace/eum166

Antzelevitch, C., and S. Sicouri. 1994. Clinical relevance of cardiac arrhythmias generated by afterdepolarizations. Role of M cells in the generation of U waves, triggered activity and torsade de pointes. *J. Am. Coll. Cardiol.* 23:259–277. http://dx.doi.org/10.1016/0735-1097(94)90529-0

Antzelevitch, C., S. Sicouri, S.H. Litovsky, A. Lukas, S.C. Krishnan, J.M. Di Diego, G.A. Gintant, and D.W. Liu. 1991. Heterogeneity within the ventricular wall. Electrophysiology and pharmacology of epicardial, endocardial, and M cells. *Circ. Res.* 69:1427–1449. http://dx.doi.org/10.1161/01.RES.69.6.1427

Asano, Y., J.M. Davidenko, W.T. Baxter, R.A. Gray, and J. Jalife. 1997. Optical mapping of drug-induced polymorphic arrhythmias and torsade de pointes in the isolated rabbit heart. *J. Am. Coll. Cardiol.* 29:831–842. http://dx.doi.org/10.1016/S0735-1097(96)00588-8

Bapat, A., T.P. Nguyen, J.H. Lee, A.A. Sovari, M.C. Fishbein, J.N. Weiss, and H.S. Karagueuzian. 2012. Enhanced sensitivity of aged fibrotic hearts to angiotensin II- and hypokalemia-induced early afterdepolarization-mediated ventricular arrhythmias. *Am. J. Physiol. Heart Circ. Physiol.* 302:H2331–H2340. http://dx.doi.org/10.1152/ajpheart.00094.2012

Catterall, W.A. 2000. Structure and regulation of voltage-gated Ca^{2+} channels. *Annu. Rev. Cell Dev. Biol.* 16:521–555. http://dx.doi.org/10.1146/annurev.cellbio.16.1.521

Chang, M.G., D. Sato, E. de Lange, J.H. Lee, H.S. Karagueuzian, A. Garfinkel, J.N. Weiss, and Z. Qu. 2012. Bi-stable wave propagation and early afterdepolarization-mediated cardiac arrhythmias. *Heart Rhythm.* 9:115–122. http://dx.doi.org/10.1016/j.hrthm.2011.08.014

Chen, P.S., T.J. Wu, C.T. Ting, H.S. Karagueuzian, A. Garfinkel, S.F. Lin, and J.N. Weiss. 2003. A tale of two fibrillations. *Circulation.* 108:2298–2303. http://dx.doi.org/10.1161/01.CIR.0000094404.26004.07

Choi, B.R., F. Burton, and G. Salama. 2002. Cytosolic Ca^{2+} triggers early afterdepolarizations and torsade de pointes in rabbit hearts with type 2 long QT syndrome. *J. Physiol.* 543:615–631. http://dx.doi.org/10.1113/jphysiol.2002.024570

Dorval, A.D., D.J. Christini, and J.A. White. 2001. Real-Time linux dynamic clamp: A fast and flexible way to construct virtual ion channels in living cells. *Ann. Biomed. Eng.* 29:897–907. http://dx.doi.org/10.1114/1.1408929

El-Sherif, N., E.B. Caref, H. Yin, and M. Restivo. 1996. The electrophysiological mechanism of ventricular arrhythmias in the long QT syndrome. Tridimensional mapping of activation and recovery patterns. *Circ. Res.* 79:474–492. http://dx.doi.org/10.1161/01.RES.79.3.474

Gotoh, Y., Y. Imaizumi, M. Watanabe, E.F. Shibata, R.B. Clark, and W.R. Giles. 1991. Inhibition of transient outward K^+ current by DHP Ca^{2+} antagonists and agonists in rabbit cardiac myocytes. *Am. J. Physiol.* 260:H1737–H1742.

Grandi, E., F.S. Pasqualini, and D.M. Bers. 2010. A novel computational model of the human ventricular action potential and Ca transient. *J. Mol. Cell. Cardiol.* 48:112–121. http://dx.doi.org/10.1016/j.yjmcc.2009.09.019

January, C.T., and J.M. Riddle. 1989. Early afterdepolarizations: mechanism of induction and block. A role for L-type Ca^{2+} current. *Circ. Res.* 64:977–990. http://dx.doi.org/10.1161/01.RES.64.5.977

January, C.T., J.M. Riddle, and J.J. Salata. 1988. A model for early afterdepolarizations: induction with the Ca^{2+} channel agonist Bay K 8644. *Circ. Res.* 62:563–571. http://dx.doi.org/10.1161/01.RES.62.3.563

Karwatowska-Prokopczuk, E., W. Wang, M.L. Cheng, D. Zeng, P.J. Schwartz, and L. Belardinelli. 2013. The risk of sudden cardiac death in patients with non-ST elevation acute coronary syndrome and prolonged QTc interval: effect of ranolazine. *Europace.* 15:429–436. http://dx.doi.org/10.1093/europace/eus400

Lin, R.J., J. Bettencourt, J. Wha Ite, D.J. Christini, and R.J. Butera. 2010. Real-time experiment interface for biological control applications. *Conf. Proc. IEEE Eng. Med. Biol. Soc.* 2010:4160–4163.

Madhvani, R.V., Y. Xie, A. Pantazis, A. Garfinkel, Z. Qu, J.N. Weiss, and R. Olcese. 2011. Shaping a new Ca^{2+} conductance to suppress early afterdepolarizations in cardiac myocytes. *J. Physiol.* 589:6081–6092. http://dx.doi.org/10.1113/jphysiol.2011.219600

Mahajan, A., Y. Shiferaw, D. Sato, A. Baher, R. Olcese, L.H. Xie, M.J. Yang, P.S. Chen, J.G. Restrepo, A. Karma, et al. 2008. A rabbit ventricular action potential model replicating cardiac dynamics at rapid heart rates. *Biophys. J.* 94:392–410. http://dx.doi.org/10.1529/biophysj.106.98160

Nitta, J., T. Furukawa, F. Marumo, T. Sawanobori, and M. Hiraoka. 1994. Subcellular mechanism for Ca^{2+}-dependent enhancement of delayed rectifier K^+ current in isolated membrane patches of guinea pig ventricular myocytes. *Circ. Res.* 74:96–104. http://dx.doi.org/10.1161/01.RES.74.1.96

Qu, Z., and D. Chung. 2012. Mechanisms and determinants of ultralong action potential duration and slow rate-dependence in cardiac myocytes. *PLoS ONE.* 7:e43587. http://dx.doi.org/10.1371/journal.pone.0043587

Qu, Z., L.H. Xie, R. Olcese, H.S. Karagueuzian, P.S. Chen, A. Garfinkel, and J.N. Weiss. 2013. Early afterdepolarizations in cardiac myocytes: beyond reduced repolarization reserve. *Cardiovasc. Res.* 99:6–15. http://dx.doi.org/10.1093/cvr/cvt104

Rose, W.C., C.W. Balke, W.G. Wier, and E. Marban. 1992. Macroscopic and unitary properties of physiological ion flux through L-type Ca^{2+} channels in guinea-pig heart cells. *J. Physiol.* 456:267–284. http://dx.doi.org/10.1113/jphysiol.1992.sp019336

Rosen, M.R. 1988. Mechanisms for arrhythmias. *Am. J. Cardiol.* 61:A2–A8. http://dx.doi.org/10.1016/0002-9149(88)90735-7

Sato, D., L.H. Xie, A.A. Sovari, D.X. Tran, N. Morita, F. Xie, H. Karagueuzian, A. Garfinkel, J.N. Weiss, and Z. Qu. 2009. Synchronization of chaotic early afterdepolarizations in the genesis of cardiac arrhythmias. *Proc. Natl. Acad. Sci. USA.* 106:2983–2988. http://dx.doi.org/10.1073/pnas.0809148106

Sato, D., L.H. Xie, T.P. Nguyen, J.N. Weiss, and Z. Qu. 2010. Irregularly appearing early afterdepolarizations in cardiac myocytes: Random fluctuations or dynamical chaos? *Biophys. J.* 99:765–773. http://dx.doi.org/10.1016/j.bpj.2010.05.019

Shiferaw, Y., M.A. Watanabe, A. Garfinkel, J.N. Weiss, and A. Karma. 2003. Model of intracellular calcium cycling in ventricular myocytes. *Biophys. J.* 85:3666–3686. http://dx.doi.org/10.1016/S0006-3495(03)74784-5

Song, Y., J.C. Shryock, S. Wagner, L.S. Maier, and L. Belardinelli. 2006. Blocking late sodium current reduces hydrogen peroxide-induced arrhythmogenic activity and contractile dysfunction. *J. Pharmacol. Exp. Ther.* 318:214–222. http://dx.doi.org/10.1124/jpet.106.101832

Tohse, N. 1990. Calcium-sensitive delayed rectifier potassium current in guinea pig ventricular cells. *Am. J. Physiol.* 258:H1200–H1207.

Tran, D.X., D. Sato, A. Yochelis, J.N. Weiss, A. Garfinkel, and Z. Qu. 2009. Bifurcation and chaos in a model of cardiac early afterdepolarizations. *Phys. Rev. Lett.* 102:258103. http://dx.doi.org/10.1103/PhysRevLett.102.258103

Verkerk, A.O., A. Baartscheer, J.R. de Groot, R. Wilders, and R. Coronel. 2011. Etiology-dependency of ionic remodeling in cardiomyopathic rabbits. *Int. J. Cardiol.* 148:154–160. http://dx.doi.org/10.1016/j.ijcard.2009.10.047

Wagner, S., H.M. Ruff, S.L. Weber, S. Bellmann, T. Sowa, T. Schulte, M.E. Anderson, E. Grandi, D.M. Bers, J. Backs, et al. 2011. Reactive oxygen species-activated Ca/calmodulin kinase IIδ is required for late I_{Na} augmentation leading to cellular Na and Ca overload. *Circ. Res.* 108:555–565. http://dx.doi.org/10.1161/CIRCRESAHA.110.221911

Ward, C.A., and W.R. Giles. 1997. Ionic mechanism of the effects of hydrogen peroxide in rat ventricular myocytes. *J. Physiol.* 500:631–642. http://dx.doi.org/10.1113/jphysiol.1997.sp022048

Weber, C.R., V. Piacentino III, K.S. Ginsburg, S.R. Houser, and D.M. Bers. 2002. Na^+-Ca^{2+} exchange current and submembrane $[Ca^{2+}]$ during the cardiac action potential. *Circ. Res.* 90:182–189. http://dx.doi.org/10.1161/hh0202.103940

Weiss, J.N., A. Garfinkel, H.S. Karagueuzian, P.S. Chen, and Z. Qu. 2010. Early afterdepolarizations and cardiac arrhythmias. *Heart Rhythm.* 7:1891–1899. http://dx.doi.org/10.1016/j.hrthm.2010.09.017

Wit, A.L., and M.R. Rosen. 1983. Pathophysiologic mechanisms of cardiac arrhythmias. *Am. Heart J.* 106:798–811. http://dx.doi.org/10.1016/0002-8703(83)90003-0

Wu, J., J. Wu, and D.P. Zipes. 2002. Early afterdepolarizations, U waves, and torsades de pointes. *Circulation.* 105:675–676.

Xie, L.H., F. Chen, H.S. Karagueuzian, and J.N. Weiss. 2009. Oxidative stress-induced afterdepolarizations and calmodulin kinase II signaling. *Circ. Res.* 104:79–86. http://dx.doi.org/10.1161/CIRCRESAHA.108.183475

Xie, Y., D. Sato, A. Garfinkel, Z. Qu, and J.N. Weiss. 2010. So little source, so much sink: Requirements for afterdepolarizations to propagate in tissue. *Biophys. J.* 99:1408–1415. http://dx.doi.org/10.1016/j.bpj.2010.06.042

Yan, G.X., Y. Wu, T. Liu, J. Wang, R.A. Marinchak, and P.R. Kowey. 2001. Phase 2 early afterdepolarization as a trigger of polymorphic ventricular tachycardia in acquired long-QT syndrome: direct evidence from intracellular recordings in the intact left ventricular wall. *Circulation.* 103:2851–2856. http://dx.doi.org/10.1161/01.CIR.103.23.2851

Yang, P.C., J. Kurokawa, T. Furukawa, and C.E. Clancy. 2010. Acute effects of sex steroid hormones on susceptibility to cardiac arrhythmias: A simulation study. *PLOS Comput. Biol.* 6:e1000658. http://dx.doi.org/10.1371/journal.pcbi.1000658

Yang, T., T.C. Atack, D.M. Stroud, W. Zhang, L. Hall, and D.M. Roden. 2012. Blocking Scn10a channels in heart reduces late sodium current and is antiarrhythmic. *Circ. Res.* 111:322–332. http://dx.doi.org/10.1161/CIRCRESAHA.112.265173

Zeng, J., and Y. Rudy. 1995. Early afterdepolarizations in cardiac myocytes: mechanism and rate dependence. *Biophys. J.* 68:949–964. http://dx.doi.org/10.1016/S0006-3495(95)80271-7